

Computational Modeling of 2D Materials under High Pressure and Their Chemical Bonding: Silicene as Possible Field-Effect Transistor

Christian Tantardini,* Alexander G. Kvashnin,* Carlo Gatti, Boris I. Yakobson, and Xavier Gonze*



Cite This: ACS Nano 2021, 15, 6861–6871



Read Online

ACCESS |

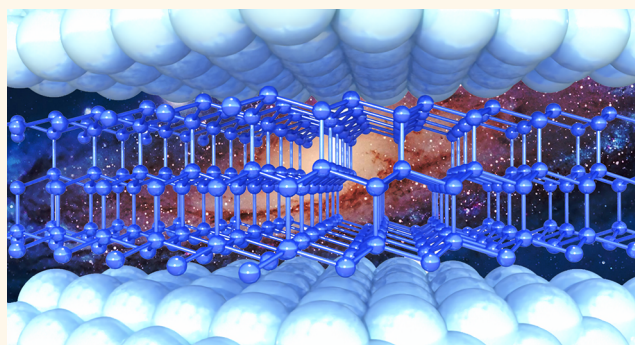
Metrics & More

Article Recommendations

Supporting Information

ABSTRACT: To study the possibility for silicene to be employed as a field-effect transistor (FET) pressure sensor, we explore the chemistry of monolayer and multilayered silicene focusing on the change in hybridization under pressure. *Ab initio* computations show that the effect of pressure depends greatly on the thickness of the silicene film, but also reveals the influence of real experimental conditions, where the pressure is not hydrostatic. For this purpose, we introduce anisotropic strain states. With pure uniaxial stress applied to silicene layers, a path for sp^3 silicon to sp^3d silicon is found, unlike with pure hydrostatic pressure. Even with mixed-mode stress (in-plane pressure half of the out-of-plane one), we find no such path. In addition to introducing our theoretical approach to study 2D materials, we show how the hybridization change of silicene under pressure makes it a good FET pressure sensor.

KEYWORDS: 2D structures, honeycomb, Abinit, silicene, field-effect transistor, pressure sensors



INTRODUCTION

Although bulk silicon (3D) is one of the most widely used chemical elements to produce modern electronic devices, the basic research on its atomic-thin 2D counterpart, silicene, is still to be completed,^{1–3} dictated by the great importance of two-dimensional (2D) materials for developing devices. This requires particular properties: (i) thin membranes, which can be deformed by in-plane stretching or by out-of-plane bending, as noted for graphene being rolled into carbon nanotubes;^{4,5} (ii) defect formation (e.g., vacancies, dislocations, grain boundaries), with special interest in how they affect the physical properties during deformation, while strength and toughness describe the onset of failure in terms of stress and energy, respectively;^{6–11} (iii) interfacial properties such as adhesion and friction, which are affected by van der Waals interactions between the surface and substrate, being 2D materials characterized by highest surface to volume ratios of any class of materials.^{12,13} Theoretically the dynamic and thermodynamic stability of multilayer silicene were exhaustively studied previously.^{14–16}

Thus, silicene seems to be promising for use in flexible, low-cost, large-scale, and lightweight electronic applications such as field-effect transistor (FET) pressure sensors. Such devices are

currently playing an important role in realizing large-area flexible and stretchable sensors.^{17,18} Typical FET pressure sensors consist of three main components: an active semiconductor layer, a dielectric (or insulator), and three terminals (*i.e.*, source, drain, and gate electrodes). Such field-effect transistor-type sensors enable easy amplification and fine-tuning of detected electrical signals by controlling the applied voltage on the third terminal, the gate electrode, in comparison with conventional sensing devices composed of only two terminals.

Sensors such as all-two-dimensional and quasi-two-dimensional materials can be modified by applying pressure. A well-known example is the transformation of multilayered graphene into diamond films (diamanes).^{19–24} This represents a fundamental understanding for material discovery. As another example, significant changes of magnetic states are seen in

Received: December 18, 2020

Accepted: March 15, 2021

Published: March 17, 2021



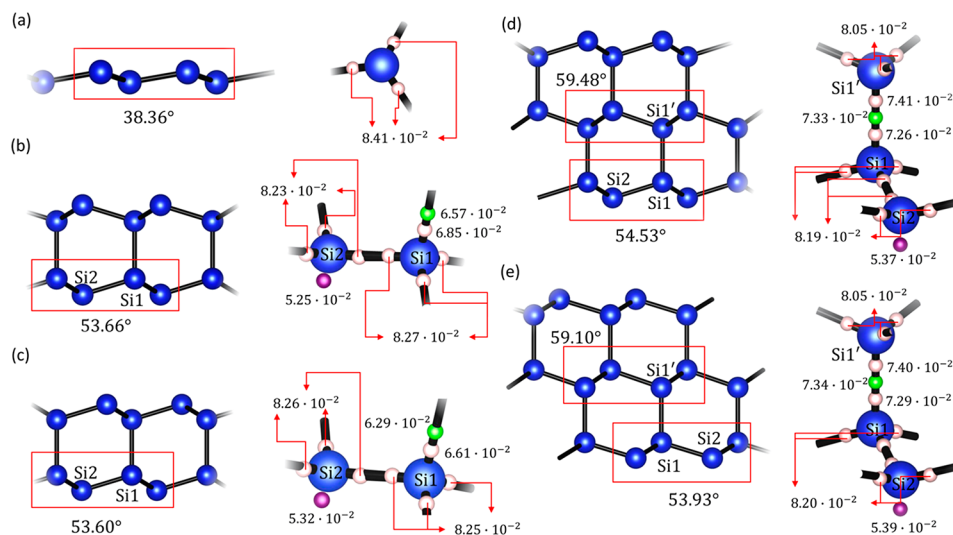


Figure 1. Atomic structure of silicene (a) monolayer, (b) AA and (c) AB bilayers, and (d) AAA and (e) ABC trilayers. Red rectangles show the atoms that the dihedral angles were calculated for. Blue color represents silicon atoms, light pink balls represent bond maxima (BM), green balls are bond critical points (BCPs), violet balls are nonbonding maxima (NBM). Numbers denote the value of electron density at specific $L = -\nabla^2\rho$ or electron density critical points in e/bohr^3 .

layered CrI_3 by application of pressure in a piston pressure cell.^{25,26} Electronic and thermoelectric properties of layered materials such as ReS_2 ²⁷ and SnSe ²⁸ can also be changed under pressure. Thus, to employ silicene thin layers for FET pressure sensors, we should comprehensively investigate changes of its electronic properties under pressure.

Such an investigation can be experimentally performed applying pressure, which is transferred to a 3D material *via* some medium, filling the environment around the sample. Usually, this medium is oil or some inert gas. During the compression, hydrostatic pressure is generated. However, in the 2D case, the situation is different. Supposing absence of the medium, anisotropic pressure will be generated, leading to free expansion of the 2D sample along the xy -plane. Moreover high and ultrahigh pressures (>10 GPa) can be achieved locally on 2D materials by using atomic force microscopy (AFM) diamond tips, as was shown in ref 29. This technique allows one to perform local changes of structure and create regions with different electronic properties located in the 2D material.

In simulations, the main issue is the correct description of pressure-induced effects, depending on the kind of boundary conditions applied on layered 2D materials. In some case the pressure is simulated by varying the interlayer distance in the perpendicular direction while keeping fixed the in-plane lattice parameter.²⁶ Here we simulate the anisotropic uniaxial pressure along the directions perpendicular to the plane of the 2D material without any artificial fixing of atomic structure, allowing the in-plane lattice parameter to vary, corresponding to zero in-plane stress. This is closer to the experimental local application of stress by an AFM. The vacuum space between periodic images of the 2D structure should be removed to simulate the pressure, with an adequate model of uniaxial stress from the AFM tip or from another medium. In this atomic-scale calculation, the choice of which atoms and how they should be placed within the unit cell is not straightforward.

In this work we have carefully considered such issues. We treat different stress states of a 2D material to which pressure is applied through inert He layers. We validate our method and explore its outcome in the study of silicene. Silicene is the two-

dimensional allotrope of silicon, having a honeycomb low-buckled structure. This material allows the easy manipulation of Dirac cones with external periodic potentials,³⁰ giving the possibility to generate exotic quantum devices. For example, applying symmetry-breaking potentials to graphene could renormalize the Fermi velocity of the Dirac bands,^{31–33} replicate the Dirac cones,^{34,35} or gap out the Dirac points.^{36–39}

Silicene has no counterparts in the bulk, at variance with graphene (*i.e.*, two-dimensional allotrope of carbon), which is more stable with respect to its bulk counterpart. Si and C atoms have similar electronic configurations with metallic band structure of their 2D honeycomb allotropes, and, for C under pressure, the sp^3 hybridization is more favorable, leading to conversion from multilayered graphene to diamanes, passing from metallic to nonmetallic band structure (*i.e.*, semiconductor).^{20,22} However, the Si hybridization in a honeycomb low-buckled state is still controversial in the literature with the assumption to be either sp^2 or sp^3 distorted: Si is expected to be sp^2 hybridized due to the metallic band structure, which is characteristic for such hybridization, but Si is also expected to be sp^3 hybridized due to lack of planar structure.

Thus, a preliminary study of electron density of silicene under vacuum could be useful to solve this issue. Furthermore, a subsequent investigation at high pressure may show the $\text{sp}^3\text{--}\text{sp}^2$ transition and/or explain how to achieve a pure sp^2 hybridization (*i.e.*, flat honeycomb), with concomitant increasing of conductivity at high pressure. It will be interesting to understand the possibility of formation of high-conductivity multilayered sp^2 -hybridized silicene at high pressure with the possibility to develop electronic devices for extreme environments.

RESULTS AND DISCUSSION

Zero Pressure Study. The initial open question that we answer is about the Si hybridization within a free-standing honeycomb monolayer. To solve it, we evaluate the critical points (CPs) of function L within the valence shell charge concentration (VSCC) region of Si atoms: a maximum of L corresponds to a local accumulation of electron density, while a minimum of L indicates a local depletion of electron density.

Thus, an analysis of VSCC for a bonded Si atom can give us an initial indication about the nature of its bonding. If a maximum CP sits along a bond path,^{40–47} it can be described as a bond maximum (BM), whereas all other maximum CPs are nonbonding maxima (NBM).^{40–47} As expected, all Si atoms in the silicene monolayer have a BM along their corresponding bond paths (light pink balls in Figure 1a), but there are no NBMs perpendicular to the xy -plane indicating the residual lone pair of the nonhybridized p_z -orbital. This initial analysis confirms a distorted sp^3 geometry instead of distorted sp^2 . To be sure, we had to understand where the fourth valence electron is located, which is not directly involved in the bond formation for a distorted sp^3 geometry. The three BMs are located at 0.78 Å from their corresponding nucleus and with an electron density value equal to 8.41×10^{-2} e/bohr³. It can be compared with the value of 5.44×10^{-2} e/bohr³ found for isolated Si on the L maximum atomic spherical surface, located at 0.75 Å from the nucleus (see Figure 1a and Table S1 in the Supporting Information). This result suggests a distorted sp^3 hybridization due to the smearing of the remaining electron around three bonds with a resulting increase in the electron density on the BMs, pulling them away from the Si nucleus relative to the isolated Si. The firm confirmation of distorted sp^3 comes from the comparison of electron density at the BM in the monolayer with that in bulk diamond-type silicon, where Si is fully sp^3 hybridized. Diamond silicon showed 8.06×10^{-2} e/bohr³ at the BMs around Si, which are located 0.77 Å from the nucleus. The lower electron density at the BMs in diamond silicon with respect to that in silicene confirms in the latter the distorted sp^3 hybridization of Si atoms.

In contrast to carbon, the silicon has only an sp^3 -hybridized bulk allotrope, which leads to the formation of low-buckled 2D silicene. Thus, it is an open question whether it is possible to create a multilayered silicene structure at high pressures.

First, we considered three types of silicene films, namely, mono-, bi-, and trilayer at zero pressure. Bi- and trilayered silicene films were considered to have the structure of previously studied diamond and lonsdaleite films with (111) and (0001) surfaces, respectively^{19,20,22,23} (Figure 1b–e). Thus, silicene films with a diamond structure have AB or ABC stacking of the layers, while AA-stacked films belong to lonsdaleite films with a (0001) surface.

The analysis of atomic structures was made in terms of dihedral angles. The dihedral angle of a monolayer of silicene is 38.36° (Figure 1a), while for AA and AB films they are equal to 54.89° and 53.60°, respectively (Figure 1b,c and Table S1 in the Supporting Information). AAA and ABC films can be represented as consisting of two types of layers: two surface layers and a middle (“bulk-like”) one (Figure 1d,e). Dihedral angles of surface layers of AAA and ABC films are 54.53° and 53.93°, while dihedral angles of middle layers of AA and ABC films equal 59.48° and 59.10°, respectively. Dihedral angles between Si atoms in the middle layers of three-layered films are similar to corresponding angles in the bulk Si (see Table S1 in the Supporting Information).

This fact indicates the increase of sp^3 hybridization of Si films with the increase of the number of layers. The silicene layers are bonded between them, and with the increase of the number of layers, the increase of sp^3 hybridization will be translated into an increase of strength of interlayer bonds. This is shown by an increase of electron density at the bond critical point (BCP) of the interlayer bond with increasing number of layers. To definitely prove that the sp^3 hybridization of Si is correlated to

the number of layers, we have searched the CPs of the L function within the VSCC region to explain the atomic hybridization of silicon atoms in the films.

The unit cells of both AA and AB films consist of two symmetrically nonequivalent Si atoms in each layer. One of the atomic types (Si1) has a coordination number of 4; another type (Si2) has only three neighbors. Atoms of Si1 type form three bonds with Si2 atoms of the same layers and one bond with the Si1 atom from the second layers (see Figure 1b,c). The interlayer bond is confirmed by the presence of a BCP with ρ equal to 6.57×10^{-2} and 6.29×10^{-2} e/bohr³, respectively, for AA and AB films (see green balls in Figure 1b,c) between two Si1 atoms of different layers.

There is an overall increase of sp^3 hybridization for silicon atoms passing from monolayer to bilayers. This is first shown by the increase of dihedral angle and subsequently by the decrease of electron density delocalization around the nucleus, as shown by the presence of Si atoms (Si1) with four BMs and by the occurrence of an NBM in Si2 atoms (see Figure 1a,b,c).

The Si2 of AB packing has a higher sp^3 hybridization with respect to an AA-stacked film due to the slightly higher uniform localization of valence electrons around Si2 atoms in the AB film (see Figure 1b,c).

For silicene films with three layers we considered AAA and ABC stackings. AAA films have two symmetrically non-equivalent Si atoms in each of the outer layers (Figure 1d,c). One of them (Si1) creates a chemical bond with the Si atom of the middle layer (Si1'), while another atom (Si2) has chemical bonds only with Si1 atoms within its layer. In the middle layer all atoms make interlayer bonds connecting with the Si1 atoms of other layers (Figure 1d,c). Thus, the involvement of Si atoms of the middle layer in four bonds guarantees that they have the same sp^3 hybridization (Si1'). The chemical bonding between the layers is confirmed by the presence of a BCP with ρ equal to 7.33×10^{-2} and 7.34×10^{-2} e/bohr³ for AAA and ABC layers, respectively (see Table S1 in the Supporting Information).

In AAA and ABC layers we found a decrease of electron density at the BMs that surround each nucleus and an increase at the NBM of Si2 with respect to bilayers (see Figure 1). This confirms the increase of electronic localization and thus an increased sp^3 hybridization of Si atoms. Furthermore, the different packing of two silicene layers (*i.e.*, ABC) seems to determine a higher sp^3 hybridization with respect to having the same packing (*i.e.*, AAA) as the valence electrons are more localized (see Figure 1d,e).

This shows that the increase of the number of layers leads to the increase of sp^3 hybridization of silicon atoms. In order to understand how these results correlate with properties of single-crystal silicon, we have considered two types of bulk silicon having AA (*i.e.*, lonsdaleite) and ABC (*i.e.*, diamond) stacking. As we know, all Si atoms in both ABC and AA silicon have sp^3 hybridization, where the BMs are located along the bond path at 0.78 Å from the nucleus. Although they are located at the same distance from the nucleus, the electron density is differently distributed between them. In lonsdaleite-type silicon the electron density at 3 BM with the Si of the same layer is slightly higher (*i.e.*, $\rho = 8.07 \times 10^{-2}$ e/bohr³) than the BM located between the layers (*i.e.*, $\rho = 7.96 \times 10^{-2}$ e/bohr³). For diamond-type silicon the electron density at 4 BM is obviously the same (*i.e.*, $\rho = 8.05 \times 10^{-2}$ e/bohr³). In periodic 3D structures the reduction of electron density at the BMs around the nucleus with respect to 2D structures shows a higher sp^3 hybridization of the Si in comparison to films. It is noteworthy that diamond Si is

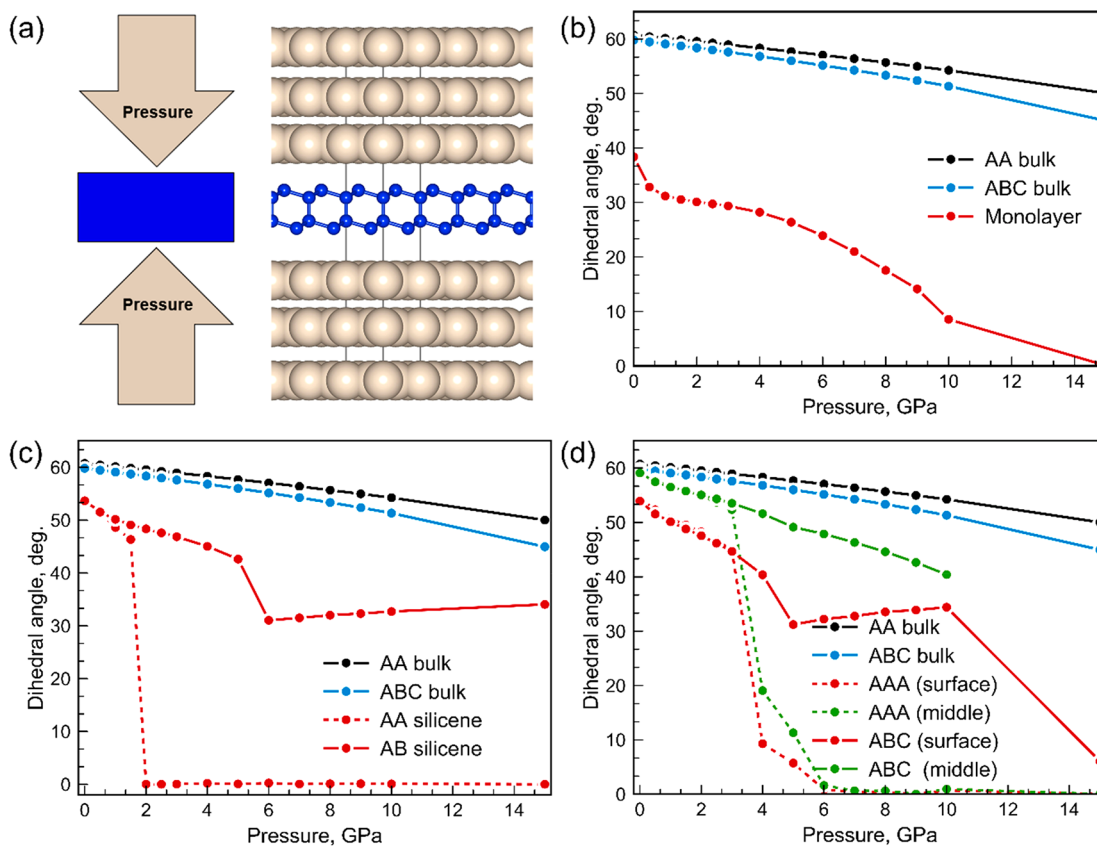


Figure 2. (a) Schematic illustration of the simulation of anisotropic compression of 2D materials. Dependence of dihedral angles on the applied pressure for (b) silicene monolayer, (c) bilayers with AA and AB stackings, and (d) ABC and AAA films in comparison with bulk diamond- and lonsdaleite-like silicon structures. The exact values are reported in Table S2 in the Supporting Information.

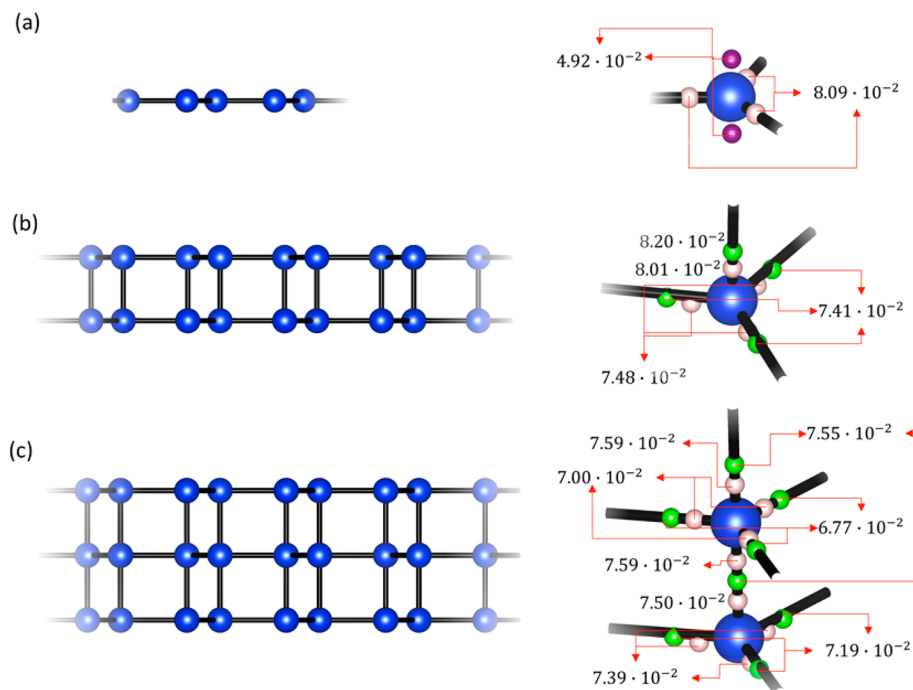


Figure 3. Atomic structure of studied silicene (a) monolayer at 15 GPa, (b) AA bilayer at 5 GPa, and (c) AAA trilayer at 15 GPa. Blue color represents silicon atoms, light pink balls represent bond maxima (BM), green balls are bond critical points (BCPs), and violet balls are nonbonding maxima (NBM). Numbers denote the value of the electron density at specific critical points in e/bohr^3 .

thermodynamically more stable than lonsdaleite-type Si. This could be associated with the homogeneous electronic

distribution around Si atoms of diamond with respect to the inhomogeneous electronic distribution around Si atoms in

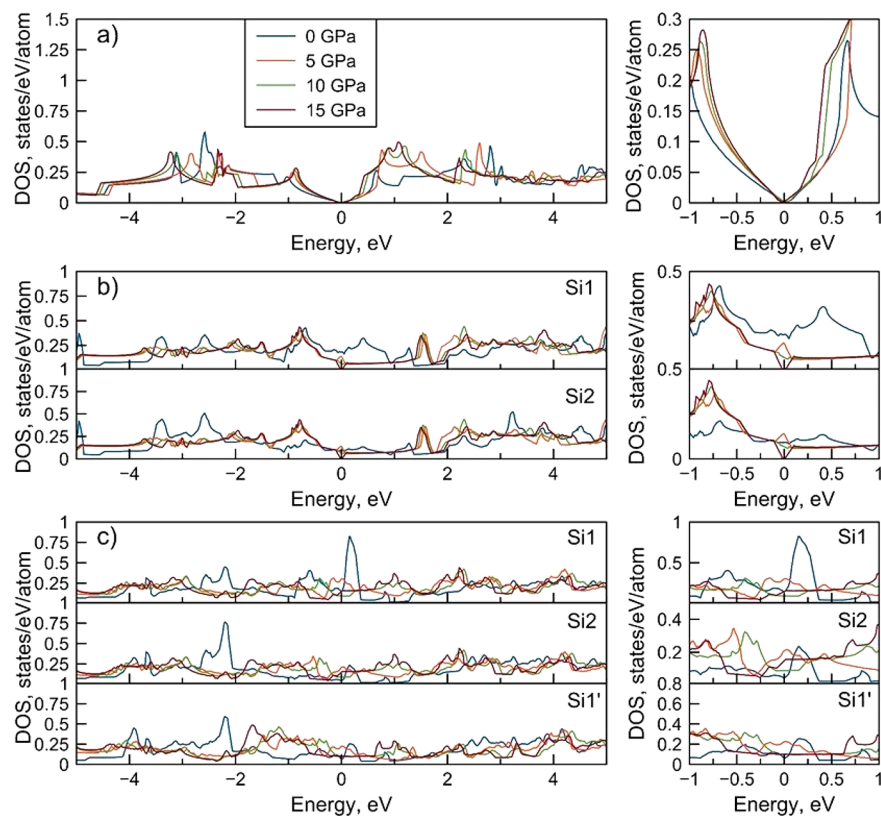


Figure 4. Density of states (DOS) of (a) monolayer, (b) AA bilayer, and (c) AAA trilayer at different values of uniaxial compression.

lonsdaleite-type silicon. Homogeneity of the electron distribution reflects the highest stability of diamond structure.

High-Pressure Study. To understand how atomic hybridization in silicene changes under pressure, we have simulated anisotropic compression of monolayers, bilayers, and trilayers replacing the vacuum with helium atoms conserving the symmetry of layers, as shown in Figure 2a.

A uniaxial pressure is able to compress the structure along the z -axis with consequent expansion in the xy -plane. This can trigger transition to planar silicene, with evolution of sp^3 hybridization of Si atoms to sp^2 . To identify such a transition, the dihedral angle is monitored under pressure (see Figure 2b–d).

The silicene monolayer, AA bilayer, and AAA trilayer are the only cases for which the pressure pushes the dihedral angle close to zero (see Figure 2c,d and Supporting Information Figure S14). Such a geometry is usually associated with sp^2 hybridization *in vacuo*, but at high pressure one must check the breaking and/or creating of bonds. A flat configuration is obtained for monolayer and AAA trilayers at 15 GPa, while for an AA bilayer at 2 GPa. At the same pressures the structures of the two bulk allotropes are practically unaffected (see Figure 2b–d).

The same symmetry of Si atoms and the uniaxial pressure guarantee the achievement of a flat silicene. If Si atoms within the unit cell have the same symmetry, they can reciprocally repel each other, preventing the Si atoms of one layer from shifting on the center of the honeycomb of the other layer due to the increasing of high pressure, as in AB and ABC layers (see Supporting Information Figure S15 and Figure S16). In the case of different layer packing with pressure it is not possible to generate a flat silicene multilayer.

The search of CPs of the L function within the VSCC of Si atoms for a silicene monolayer at 15 GPa shows the presence of two NBM perpendicular to the plane of the three BMs (see Figure 3a). The values of electron density at BMs are almost twice as large in comparison with electron density at NBMs showing a perfect sp^2 hybridization of the silicene monolayer. For bilayered AA silicene we confirm the presence of interlayer bonds by calculations of interlayer BCPs (green balls in Figure 3b). The study of the electron distribution around the Si atom shows 4 BM, and 3 of them, those in the plane of the layer, are displaced from the bond path, as are the BCPs, suggesting a geometric strain to be present. This also means that at high pressure the intralayer bonds become weaker than interlayer bonds, as supported also by the lower electron density of the former at the BMs (see Figure 3b). In this case, Si retains a distorted sp^3 hybridization instead of converting from sp^3 to sp^2 . In the case of AAA trilayers the Si atoms that belong to the outer layers have the same distorted sp^3 hybridization as for the AA silicene film, but the Si atoms of the middle layer become 5-fold coordinated (Figure 3c). This should be possible due to the high pressure that makes the empty d-orbitals available, generating an sp^3d hybridization (*i.e.*, trigonal bipyramidal geometry). This kind of hybridization is possible for Si atoms having a $3s^23p^2$ valence configuration. Thus, it has available 3d-orbitals, while a carbon atom with a $2s^22p^2$ valence configuration has no available d-orbitals with the same principal quantum number of its occupied valence orbitals. For this reason, at high pressure a multilayer graphene will be converted into a diamond structure, while silicene at high pressure is not converted into diamond-like structure because the alternative and available sp^3d hybridization is energetically more favorable than sp^3 .

For a silicon monolayer and AA and AAA layered films we have performed calculations of the electronic density of states

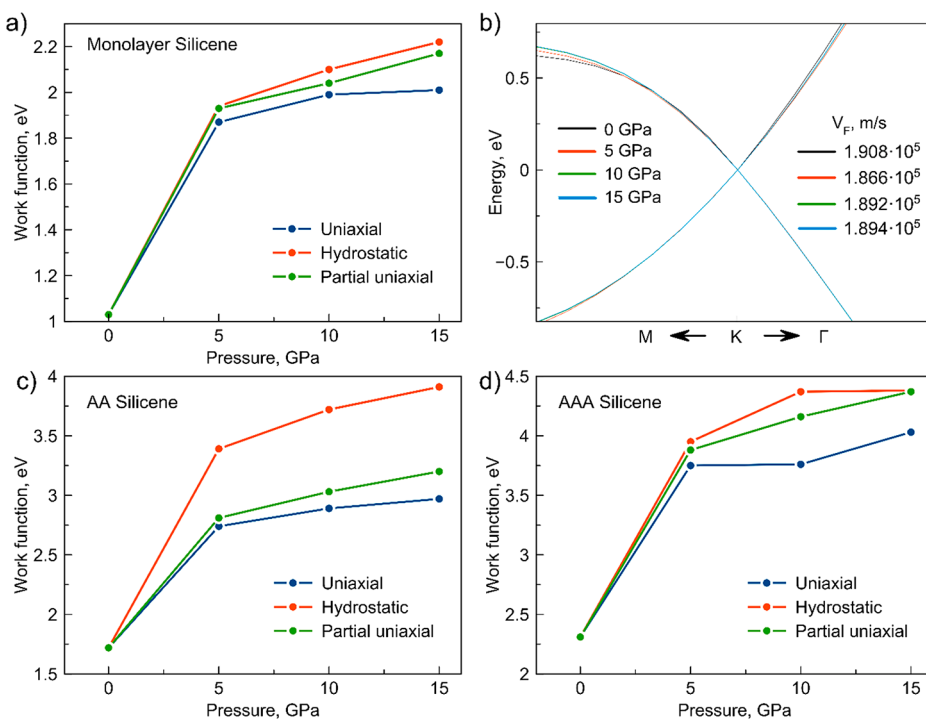


Figure 5. Work function for (a) monolayer, (c) AA bilayer, and (d) AAA trilayer, as a function of pressure for different types of compression; (b) monolayer band structures at different pressures (uniaxial compression) around the K-point with an indication of Fermi velocity. Dirac cones were shifted to the Fermi energy as a reference.

(DOS) as a function of uniaxial pressure (see Figure 4 and, for more details, Supporting Information Figures S2 to S12). The dependence of the work function on the pressure is shown in the Supporting Information (Table S4 and Figure S13). This information allows one to see how the changes of hybridization from sp^3 to sp^2 in the case of a monolayer (sp^3 to sp^3d in the case of 2 and 3 layered films) will affect electronic properties. Increasing the pressure leads to an increase of the slope of the Dirac cone (Figure 4a). More significant changes of electronic DOS were observed for the AA silicon film as it undergoes complete structure changes (Figure 4b). In this case the sp^3 hybridization of silicon atoms changes to sp^3d . At 0 GPa the DOS of Si1 and Si2 atoms differ from each other, as the atoms are symmetrically inequivalent and have different numbers of chemical bonds. Pressure increases lead to equality of DOS for both atoms (Figure 4b). The structure of the film becomes flat, and Si1 and Si2 atoms become symmetrically equivalent. A similar situation is observed in the case of an AAA silicon film (Figure 4c), where uniaxial compression leads to changes of hybridization from sp^3 to sp^3d . This structure becomes flat at a pressure higher than 15 GPa.

At the end of this work, we simulate the experimental conditions that might be present in the diamond anvil cells. To do this, we have partially compressed the xy -plane by half of the applied pressure along the z -axes and compared the dihedral angle previously obtained for a full uniaxial pressure along the z -axes. We have also compared these results with those obtained by applying hydrostatic pressure performed by us. Initially, we have investigated monolayer silicene, and the results showed the impossibility to obtain flat monolayer silicene when we do not apply full uniaxial pressure. This is reflected in the DOS on changing the conductivity (see Figure S1 in the Supporting Information). Furthermore, we have investigated the band structures of monolayers, AA bilayers, and AAA trilayers (see

Supporting Information Figures S17–S19). The silicene monolayer showed Dirac cones in the K-point of the Brillouin zone similar to those that are seen in a graphene monolayer, and the Fermi velocity that we have measured is on the order of $\sim 10^5$ m/s, in line with literature results^{48–50} and of 1 order of magnitude smaller than Fermi velocity of a graphene monolayer (*i.e.*, $\sim 10^6$ m/s), also with pressure (see Figure 5b).

Detailed examination of the band structures of the AA bilayer and AAA trilayer (see Supporting Information Figures S18 and S19) reveals that for the AA bilayer under pressure the top of the valence band and the bottom of the conduction band close to Fermi level are clear (this means that they are not crossed by other bands close to the Fermi level). Thus, we estimated their overlap (see Supporting Information Table S6), which is seen to decrease with pressure from 0.1632 eV at 5 GPa to 0.0526 eV at 15 GPa. At variance, the band structure of the AAA trilayer at different pressure close to the Fermi level is quite complicated, and a simple analysis is not possible. Anyhow, we have then considered the work function, which is defined as the difference between the electrostatic potential under vacuum and the Fermi energy ($W = V - E_F$), as a function of different types of pressure for monolayer, AA, and AAA films (see Figure 5, while the respective values are shown in Supporting Information Table S5). Silicene shows an increasing W with pressure for different layers (see Figure 5). Indeed, in the middle layer of AAA three-layer the full change of silicon hybridization from sp^3 to sp^3d at 15 GPa determines a rapid increase of W . Similar increase of W makes silicene multilayer feasible to be used as an FET pressure sensor.

Since the electronic DOS of monolayer silicene is highly sensitive to applied compression, we have also studied the evolution of the DOS for AA and AAA silicene films at different pressure conditions, as these structures are the most realistic from the experimental point of view.

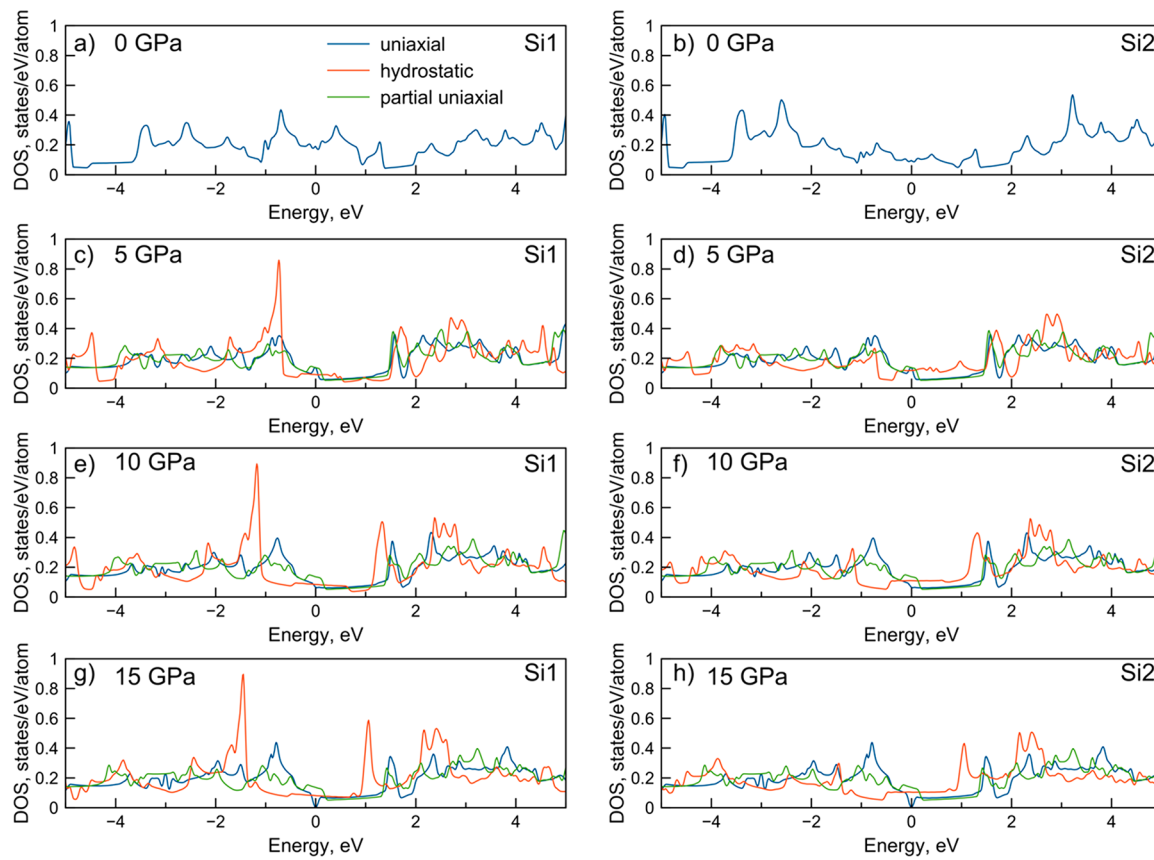


Figure 6. Evolution of electronic density of states (DOS) of AA silicene films for symmetrially nonequivalent atoms with different pressures as well as with different pressure types: uniaxial (blue), partial uniaxial (orange), and hydrostatic (green).

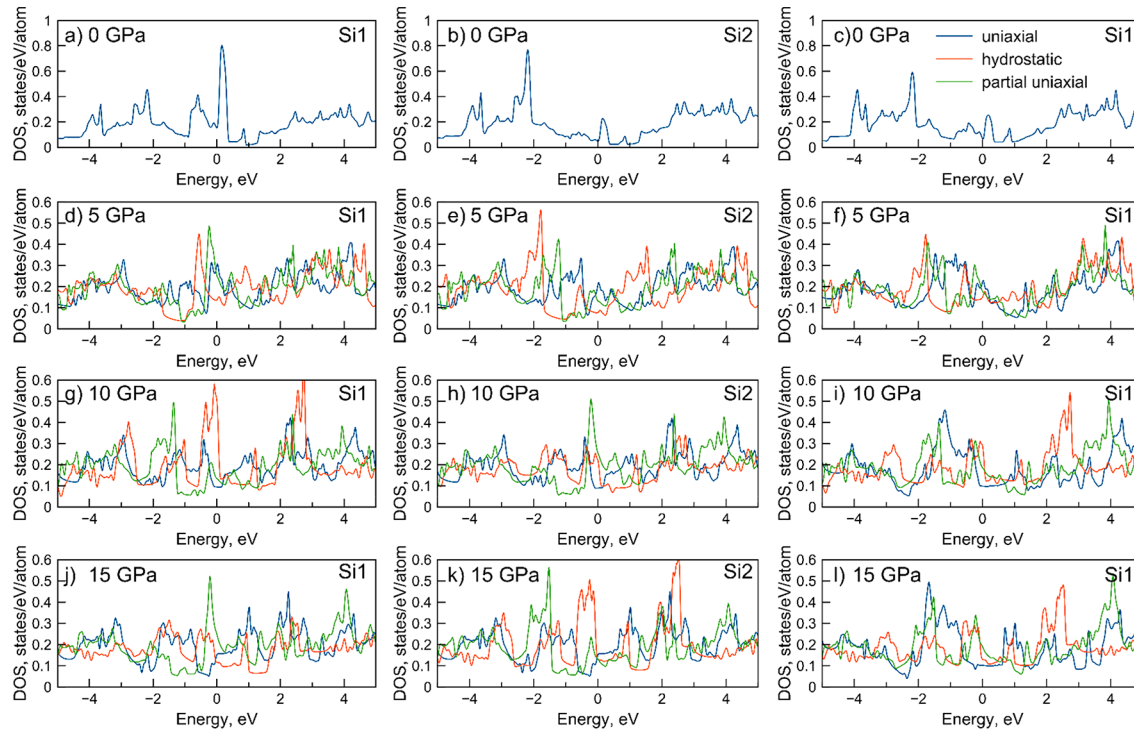


Figure 7. Evolution of electronic density of states (DOS) of AAA silicene films for symmetrially nonequivalent atoms with different pressures as well as with different pressure types: uniaxial (blue), partial uniaxial (orange), and hydrostatic (green).

As shown previously, uniaxial compression transforms both AA and AAA layers to flat multilayered films, but this is not

observed when we apply partial uniaxial and hydrostatic pressures. For the AA layer the number of nonequivalent

atoms is reduced from two to one under uniaxial compression. This is shown also by the DOS (see Figure 6 and Supporting Information Figures S7, S8, and S9), where one can see that DOS for Si1 and Si2 atoms becomes similar starting from 5 GPa, because the AA is flat already at 2 GPa. This is not observed in the case of partial uniaxial and hydrostatic types of compression (orange and green colors in Figure 5), giving a different conclusion.

For the AAA film the number of nonequivalent atoms is reduced from three to two under uniaxial compression (the structure becomes flat). In the case of a uniaxial pressure of 15 GPa the AAA film is completely flat and the DOS of Si1 and Si2 atoms becomes similar due to the fact that they have distorted sp^3 hybridization, while Si1' has an sp^3d hybridization, thus a different DOS with respect to the other two (see Figure 7 and Supporting Information Figures S10, S11, and S12). Partial uniaxial and hydrostatic compression types do not lead to such behavior of the DOS (see orange and green colors in Figure 7).

The different behavior of the electronic DOS will influence the conductivity of the films. Such behaviors for uniaxial (*i.e.*, our approach), partial uniaxial (*i.e.*, diamond anvil cell), and hydrostatic compression confirmed the validity of our approach to assess how a 2D material responds to pressure on a surface, filling the gap of currently available experimental techniques.

CONCLUSION

Our approach has shown that anisotropic pressure can be fruitfully employed to study 2D materials under pressure, for different experimental settings. Removing the vacuum can be done by adding atoms of an inert gas such as helium. Such a buffer layer can be arranged to preserve the symmetry of the studied 2D materials to simplify calculations, being inert anyhow.

The study of electron density of silicene (monolayer and multilayers) within Bader's theory, *in vacuo* and under pressure, allowed us to understand the Si hybridization as a function of pressure. This study explained that multilayer silicene is more stable with pressure due to the availability of d-orbitals passing the Si hybridization from sp^3 to sp^3d . At variance, the counterpart graphene converts to diamond due to the unavailability of d-orbitals for carbon. This mean that silicene thin films can successfully be employed as FET pressure sensors due to the variation of electronic distribution and generated charge displacement (piezoelectronic property). Silicene can be extensively employed as pressure-sensitive materials also due to the low-cost processing technologies such as large-area manufacturing technology. Thus, silicene thin films will provide an ideal solution for realizing practical FET-based pressure sensors.

METHOD AND COMPUTATIONAL DETAILS

In our work we optimize the cell parameters and atomic positions under fixed anisotropic stress. Such stress can be either hydrostatic, purely uniaxial, or with residual in-plane stress accompanying the dominant out-of-plane stress. The stress tensor, σ , with components $\sigma_{\alpha\beta}$, is obtained using the stress theorem⁵¹ and is written explicitly as

$$\sigma_{\alpha\beta} = \frac{1}{\Omega} \frac{\partial E}{\partial \epsilon_{\alpha\beta}}$$

where Ω is the primitive cell volume, E is the energy per cell, and $\epsilon_{\alpha\beta}$ is the Cauchy infinitesimal strain tensor. The Broyden–

Fletcher–Goldfarb–Shanno (BFGS) optimization algorithm^{52–55} is used to find the primitive cell and atomic positions that deliver that target stress. A smearing scheme applied to the electronic kinetic energy allows one to get smooth energy curves as a function of lattice parameters and angles.^{56–58} Norm-conserving pseudopotentials^{59,60} are chosen with respect to the projector augmented wave (PAW) function.^{61,62} This choice allows us to avoid overlap between the pseudopotential spheres of different atoms under pressure.

At the beginning we build the initial guess structure with one, two, and three monolayers of Si, leaving enough space to generate three layers of atomic He (thickness of the He layer is 10 Å) generated while preserving the trigonal geometry for the primitive silicene cell, with a P3 space group. Thin films containing two and three layers of silicon were considered to have different stackings: AA and AB for bilayers of Si (diamond and lonsdaleite types of structures) and AAA and ABC for trilayered films. We apply pressure along the z-axis to all 2D and 3D structures from 0 to 15 GPa (*i.e.*, 0.5, 1, 1.5, 2.0, 2.5, 3, 4, 5, 6, 7, 8, 9, 10, 15 GPa) with different in-plane stress states (hydrostatic, zero stress, or half the z-stress) and fully optimize the geometry at each step. The last optimized geometry of the previous step is the input for the next pressure step. To study the evolution of electronic properties with pressure due to the change of Si hybridization, we calculate the electronic DOS of optimized layers at each step and compare them with the DOS of bulk silicon (with both diamond and lonsdaleite structures). The DOS is obtained using the same level of theory employed during the optimization through the tetrahedron method for Brillouin zone integration⁶³ using Γ -centered $48 \times 48 \times 4$ wavevector meshes. Furthermore, for the layers for which we have computed the DOS we have also computed band structures at different pressures using the same level of theory and Γ -centered $6 \times 6 \times 2$ wavevector meshes, producing band structures for the Brillouin zone path Γ –M–K– Γ .

From 0 to 15 GPa we have analyzed the Laplacian of electron density within Bader's theory to evaluate the initial Si hybridization.^{44,45,64–69} We searched the CPs^{40–47} of function $L = -\nabla^2\rho$ in the valence shell charge concentration to determine the atomic hybridization based on electron density distribution. Subsequently, we performed the same analysis at high pressure, only for the flat layers, to verify the achievement of ideal sp^2 hybridization of Si with pressure.

Structure relaxations and total energy calculations were performed using the norm-conserving (NC) pseudopotentials^{59,60} and the generalized gradient approximation (GGA) using the Perdew–Burke–Ernzerhof (PBE) exchange–correlation density functional⁷⁰ as implemented in Abinit ver. 9.0.4.⁷¹ The NC pseudopotentials with four and two valence electrons for silicene and helium, respectively, were used to describe the electron–ion interactions. The optimization convergence cutoff is 5.0×10^{-5} Ha/bohr for the maximum net force on atoms, while the self-consistent-field convergence criterion is based on the residual potential cutoff equal to 10^{-12} Ha. A plane wave energy cutoff of 50 Ha and a Fermi–Dirac smearing of electronic occupations equal to 0.001 Ha ensured the convergence of total energies. The Γ -centered k-point meshes of $6 \times 6 \times 2$ for silicene films and $6 \times 6 \times 6$ for bulk silicon were used for Brillouin zone sampling. The crystal structures were visualized using VESTA software.⁷² Bader's analysis was performed using the CRITIC2 program.⁷³

ASSOCIATED CONTENT

Supporting Information

The Supporting Information is available free of charge at <https://pubs.acs.org/doi/10.1021/acsnano.0c10609>.

Details of the atomic structure of studied silicene films, electronic properties, atomic structures under uniaxial compression, and band structures of considered films under uniaxial compression ([PDF](#))

AUTHOR INFORMATION

Corresponding Authors

Christian Tantardini – Skolkovo Institute of Science and Technology, 121025 Moscow, Russian Federation; Institute of Solid State Chemistry and Mechanochemistry SB RAS, 630128 Novosibirsk, Russian Federation;  orcid.org/0000-0002-2412-9859; Email: christiantantardini@ymail.com

Alexander G. Kvashnin – Skolkovo Institute of Science and Technology, 121025 Moscow, Russian Federation;  orcid.org/0000-0002-0718-6691; Email: a.kvashnin@skoltech.ru

Xavier Gonze – Skolkovo Institute of Science and Technology, 121025 Moscow, Russian Federation; Université Catholique de Louvain, 1348 Ottignies-Louvain-la-Neuve, Belgium;  orcid.org/0000-0002-8377-6829; Email: xavier.gonze@uclouvain.be

Authors

Carlo Gatti – CNR - Consiglio Nazionale delle Ricerche, SCITEC - Istituto di Scienze e Tecnologie Chimiche "Giulio Natta", 20133 Milan, Italy

Boris I. Yakobson – Department of Chemistry, Taif University, Taif 26571, Saudi Arabia; Department of Materials Science and NanoEngineering and the Smalley Institute for Nanoscale Science and Technology, Rice University, Houston, Texas 77005, United States;  orcid.org/0000-0001-8369-3567

Complete contact information is available at:

<https://pubs.acs.org/10.1021/acsnano.0c10609>

Notes

The authors declare no competing financial interest.

ACKNOWLEDGMENTS

The authors would like to thank the Russian Science Foundation (grant 19-72-30043). The Siberian Branch of the Russian Academy of Sciences (SB RAS) Siberian Supercomputer Center is gratefully acknowledged for providing supercomputer facilities. Work at Rice University, A.G.K. at early stage and B.I.Y., was supported by the US Office of Naval Research (grant N00014-19-1-2191).

REFERENCES

- (1) Takeda, K.; Shiraishi, K. Theoretical Possibility of Stage Corrugation in Si and Ge Analogs of Graphite. *Phys. Rev. B: Condens. Matter Mater. Phys.* **1994**, *50* (20), 14916–14922.
- (2) Guzmán-Verri, G. G.; Lew Yan Voon, L. C. Electronic Structure of Silicon-Based Nanostructures. *Phys. Rev. B: Condens. Matter Mater. Phys.* **2007**, *76* (7), 075131.
- (3) Vogt, P.; De Padova, P.; Quaresima, C.; Avila, J.; Frantzeskakis, E.; Asensio, M. C.; Resta, A.; Ealet, B.; Le Lay, G. Silicene: Compelling Experimental Evidence for Graphenelike Two-Dimensional Silicon. *Phys. Rev. Lett.* **2012**, *108*, 155501.
- (4) Scidà, A.; Haque, S.; Treossi, E.; Robinson, A.; Smerzi, S.; Ravesi, S.; Borini, S.; Palermo, V. Application of Graphene-Based Flexible
- (5) Han, E.; Yu, J.; Annevelink, E.; Son, J.; Kang, D. A.; Watanabe, K.; Taniguchi, T.; Ertekin, E.; Huang, P. Y.; van der Zande, A. M. Ultrasoft Slip-Mediated Bending in Few-Layer Graphene. *Nat. Mater.* **2020**, *19* (3), 305–309.
- (6) de Souza, F. A. L.; Amorim, R. G.; Prasongkit, J.; Scopel, W. L.; Scheicher, R. H.; Rocha, A. R. Topological Line Defects in Graphene for Applications in Gas Sensing. *Carbon* **2018**, *129*, 803–808.
- (7) Jafri, S. H. M.; Carva, K.; Widenkvist, E.; Blom, T.; Sanyal, B.; Fransson, J.; Eriksson, O.; Jansson, U.; Grennberg, H.; Karis, O.; Quinlan, R. A.; Holloway, B. C.; Leifer, K. Conductivity Engineering of Graphene by Defect Formation. *J. Phys. D: Appl. Phys.* **2010**, *43* (4), 045404.
- (8) Banhart, F.; Kotakoski, J.; Krasheninnikov, A. V. Structural Defects in Graphene. *ACS Nano* **2011**, *5* (1), 26–41.
- (9) Skowron, S.; Lebedeva, I.; Popov, A.; Bichoutskaia, E. Energetics of Atomic Scale Structure Changes in Graphene. *Chem. Soc. Rev.* **2015**, *44* (10), 3143–3176.
- (10) Kvashnin, A. G.; Sorokin, P. B.; Kvashnin, D. G. The Theoretical Study of Mechanical Properties of Graphene Membranes. *Fullerenes, Nanotubes, Carbon Nanostruct.* **2010**, *18* (4–6), 497–500.
- (11) Kvashnin, D. G.; Sorokin, P. B. Effect of Ultrahigh Stiffness of Defective Graphene from Atomistic Point of View. *J. Phys. Chem. Lett.* **2015**, *6* (12), 2384–2387.
- (12) Wang, L.; Zhou, X.; Ma, T.; Liu, D.; Gao, L.; Li, X.; Zhang, J.; Hu, Y.; Wang, H.; Dai, Y.; Luo, J. Superlubricity of a Graphene/MoS₂ Heterostructure: A Combined Experimental and DFT Study. *Nanoscale* **2017**, *9* (30), 10846–10853.
- (13) Nutting, D.; Felix, J. F.; Tillotson, E.; Shin, D.-W.; De Sanctis, A.; Chang, H.; Cole, N.; Russo, S.; Woodgate, A.; Leontis, I.; Fernández, H. A.; Craciun, M. F.; Haigh, S. J.; Withers, F. Heterostructures Formed through Abraded van der Waals Materials. *Nat. Commun.* **2020**, *11* (1), 3047.
- (14) Roome, N. J.; Carey, J. D. Beyond Graphene: Stable Elemental Monolayers of Silicene and Germanene. *ACS Appl. Mater. Interfaces* **2014**, *6* (10), 7743–7750.
- (15) Padilha, J. E.; Pontes, R. B. Free-Standing Bilayer Silicene: The Effect of Stacking Order on the Structural, Electronic, and Transport Properties. *J. Phys. Chem. C* **2015**, *119* (7), 3818–3825.
- (16) Qian, C.; Li, Z. Multilayer Silicene: Structure, Electronics, and Mechanical Property. *Comput. Mater. Sci.* **2020**, *172*, 109354.
- (17) Wang, T.; Ouyang, Z.; Wang, F.; Liu, Y. A Review on Graphene Strain Sensors Based on Fiber Assemblies. *SN Appl. Sci.* **2020**, *2* (5), 862.
- (18) Tung, T. T.; Nine, M. J.; Krebsz, M.; Pasinszki, T.; Coghlani, C. J.; Tran, D. N. H.; Losic, D. Recent Advances in Sensing Applications of Graphene Assemblies and Their Composites. *Adv. Funct. Mater.* **2017**, *27* (46), 1702891.
- (19) Chernozatonskii, L. A.; Sorokin, P. B.; Kvashnin, A. G.; Kvashnin, D. G. Diamond-like C₂H Nanolayer, Diamane: Simulation of the Structure and Properties. *JETP Lett.* **2009**, *90* (2), 134–138.
- (20) Chernozatonskii, L. A.; Sorokin, P. B.; Kuzubov, A. A.; Sorokin, B. P.; Kvashnin, A. G.; Kvashnin, D. G.; Avramov, P. V.; Yakobson, B. I. Influence of Size Effect on the Electronic and Elastic Properties of Diamond Films with Nanometer Thickness. *J. Phys. Chem. C* **2011**, *115* (1), 132–136.
- (21) Odkhuu, D.; Shin, D.; Ruoff, R. S.; Park, N. Conversion of Multilayer Graphene into Continuous Ultrathin Sp₃-Bonded Carbon Films on Metal Surfaces. *Sci. Rep.* **2013**, *3* DOI: [10.1038/srep03276](https://doi.org/10.1038/srep03276).
- (22) Kvashnin, A. G.; Chernozatonskii, L. A.; Yakobson, B. I.; Sorokin, P. B. Phase Diagram of Quasi-Two-Dimensional Carbon, From Graphene to Diamond. *Nano Lett.* **2014**, *14*, 676–681.
- (23) Kvashnin, A. G.; Sorokin, P. B. Lonsdaleite Films with Nanometer Thickness. *J. Phys. Chem. Lett.* **2014**, *5*, 541–548.
- (24) Ke, F.; Zhang, L.; Chen, Y.; Yin, K.; Wang, C.; Tzeng, Y.-K.; Lin, Y.; Dong, H.; Liu, Z.; Tse, J. S.; Mao, W. L.; Wu, J.; Chen, B. Synthesis of Atomically Thin Hexagonal Diamond with Compression. *Nano Lett.* **2020**, *20* (8), 5916–5921.

- (25) Song, T.; Fei, Z.; Yankowitz, M.; Lin, Z.; Jiang, Q.; Hwangbo, K.; Zhang, Q.; Sun, B.; Taniguchi, T.; Watanabe, K.; McGuire, M. A.; Graf, D.; Cao, T.; Chu, J.-H.; Cobden, D. H.; Dean, C. R.; Xiao, D.; Xu, X. Switching 2D Magnetic States via Pressure Tuning of Layer Stacking. *Nat. Mater.* **2019**, *18* (12), 1298–1302.
- (26) Li, T.; Jiang, S.; Sivadas, N.; Wang, Z.; Xu, Y.; Weber, D.; Goldberger, J. E.; Watanabe, K.; Taniguchi, T.; Fennie, C. J.; Fai Mak, K.; Shan, J. Pressure-Controlled Interlayer Magnetism in Atomically Thin CrI₃. *Nat. Mater.* **2019**, *18* (12), 1303–1308.
- (27) Oliva, R.; Laurien, M.; Dybala, F.; Kopaczek, J.; Qin, Y.; Tongay, S.; Rubel, O.; Kudrawiec, R. Pressure Dependence of Direct Optical Transitions in ReS₂ and ReSe₂. *npj 2D Mater. Appl.* **2019**, *3* (1), 1–8.
- (28) Nishimura, T.; Sakai, H.; Mori, H.; Akiba, K.; Usui, H.; Ochi, M.; Kuroki, K.; Miyake, A.; Tokunaga, M.; Uwatoko, Y.; Katayama, K.; Murakawa, H.; Hanasaki, N. Large Enhancement of Thermoelectric Efficiency Due to a Pressure-Induced Lifshitz Transition in SnSe. *Phys. Rev. Lett.* **2019**, *122* (22), 226601.
- (29) Ares, P.; Pisarra, M.; Segovia, P.; Díaz, C.; Martín, F.; Michel, E. G.; Zamora, F.; Gómez-Navarro, C.; Gómez-Herrero, J. Tunable Graphene Electronics with Local Ultrahigh Pressure. *Adv. Funct. Mater.* **2019**, *29* (8), 1806715.
- (30) Feng, B.; Zhou, H.; Feng, Y.; Liu, H.; He, S.; Matsuda, I.; Chen, L.; Schwier, E. F.; Shimada, K.; Meng, S.; Wu, K. Superstructure-Induced Splitting of Dirac Cones in Silicene. *Phys. Rev. Lett.* **2019**, *122* (19), 196801.
- (31) Park, C.-H.; Yang, L.; Son, Y.-W.; Cohen, M. L.; Louie, S. G. Anisotropic Behaviours of Massless Dirac Fermions in Graphene under Periodic Potentials. *Nat. Phys.* **2008**, *4* (3), 213–217.
- (32) Rusponi, S.; Papagno, M.; Moras, P.; Vlaic, S.; Etzkorn, M.; Sheverdyeva, P. M.; Pacilé, D.; Brune, H.; Carbone, C. Highly Anisotropic Dirac Cones in Epitaxial Graphene Modulated by an Island Superlattice. *Phys. Rev. Lett.* **2010**, *105* (24), 246803.
- (33) Zou, Q.; Belle, B. D.; Zhang, L. Z.; Xiao, W. D.; Yang, K.; Liu, L. W.; Wang, G. Q.; Fei, X. M.; Huang, Y.; Ma, R. S.; Lu, Y.; Tan, P. H.; Guo, H. M.; Du, S. X.; Gao, H.-J. Modulation of Fermi Velocities of Dirac Electrons in Single Layer Graphene by Moiré Superlattice. *Appl. Phys. Lett.* **2013**, *103* (11), 113106.
- (34) Park, C.-H.; Yang, L.; Son, Y.-W.; Cohen, M. L.; Louie, S. G. New Generation of Massless Dirac Fermions in Graphene under External Periodic Potentials. *Phys. Rev. Lett.* **2008**, *101* (12), 126804.
- (35) Barbier, M.; Vasilopoulos, P.; Peeters, F. M. Extra Dirac Points in the Energy Spectrum for Superlattices on Single-Layer Graphene. *Phys. Rev. B: Condens. Matter Mater. Phys.* **2010**, *81* (7), 075438.
- (36) Pletikosić, I.; Kralj, M.; Pervan, P.; Brako, R.; Coraux, J.; N'Diaye, A. T.; Busse, C.; Michely, T. Dirac Cones and Minigaps for Graphene on Ir(111). *Phys. Rev. Lett.* **2009**, *102* (5), 056808.
- (37) Liu, W.; Wang, Z. F.; Shi, Q. W.; Yang, J.; Liu, F. Band-Gap Scaling of Graphene Nanohole Superlattices. *Phys. Rev. B: Condens. Matter Mater. Phys.* **2009**, *80* (23), 233405.
- (38) Dvorak, M.; Oswald, W.; Wu, Z. Bandgap Opening by Patterning Graphene. *Sci. Rep.* **2013**, *3* (1), 2289.
- (39) Song, J. C. W.; Shytov, A. V.; Levitov, L. S. Electron Interactions and Gap Opening in Graphene Superlattices. *Phys. Rev. Lett.* **2013**, *111* (26), 266801.
- (40) Bader, R. F. W.; Essén, H. The Characterization of Atomic Interactions. *J. Chem. Phys.* **1984**, *80* (5), 1943–1960.
- (41) Bader, R. F. W. *Atoms in Molecules: A Quantum Theory*; International Series of Monographs on Chemistry; Oxford University Press: Oxford, NY, 1994.
- (42) Gatti, C. Challenging Chemical Concepts through Charge Density of Molecules and Crystals. *Phys. Scr.* **2013**, *87* (4), 048102.
- (43) Schmøkkel, M. S.; Cenedese, S.; Overgaard, J.; Jørgensen, M. R. V.; Chen, Y.-S.; Gatti, C.; Stalke, D.; Iversen, B. B. Testing the Concept of Hypervalency: Charge Density Analysis of K₂SO₄. *Inorg. Chem.* **2012**, *51* (15), 8607–8616.
- (44) Tantardini, C.; Boldyreva, E. V.; Benassi, E. Hypervalency in Organic Crystals: A Case Study of the Oxicam Sulfonamide Group. *J. Phys. Chem. A* **2016**, *120* (51), 10289–10296.
- (45) Tantardini, C.; Benassi, E. Crystal Structure Resolution of an Insulator Due to the Cooperative Jahn–Teller Effect through Bader's Theory: The Challenging Case of Cobaltite Oxide Y114. *Dalton Trans.* **2018**, *47* (15), 5483–5491.
- (46) Gatti, C. Chemical Bonding in Crystals: New Directions. *Z. Kristallogr. - Cryst. Mater.* **2005**, *220* (5–6), 399–457.
- (47) Gatti, C. The Source Function Descriptor as a Tool to Extract Chemical Information from Theoretical and Experimental Electron Densities. In *Electron Density and Chemical Bonding II: Theoretical Charge Density Studies*; Stalke, D., Ed.; Structure and Bonding; Springer: Berlin, Heidelberg, 2012; pp 193–285 DOI: [10.1007/430_2010_31](https://doi.org/10.1007/430_2010_31).
- (48) Qin, R.; Wang, C.-H.; Zhu, W.; Zhang, Y. First-Principles Calculations of Mechanical and Electronic Properties of Silicene under Strain. *AIP Adv.* **2012**, *2* (2), 022159.
- (49) Huang, S.; Kang, W.; Yang, L. Electronic Structure and Quasiparticle Bandgap of Silicene Structures. *Appl. Phys. Lett.* **2013**, *102* (13), 133106.
- (50) Chowdhury, S.; Jana, D. A Theoretical Review on Electronic, Magnetic and Optical Properties of Silicene. *Rep. Prog. Phys.* **2016**, *79* (12), 126501.
- (51) Nielsen, O. H.; Martin, R. M. Quantum-Mechanical Theory of Stress and Force. *Phys. Rev. B: Condens. Matter Mater. Phys.* **1985**, *32* (6), 3780–3791.
- (52) Broyden, C. G. The Convergence of a Class of Double-Rank Minimization Algorithms 1. General Considerations. *IMA J. Appl. Math.* **1970**, *6* (1), 76–90.
- (53) Goldfarb, D. A Family of Variable-Metric Methods Derived by Variational Means. *Math. Comp.* **1970**, *24* (109), 23–26.
- (54) Shanno, D. F. Conditioning of Quasi-Newton Methods for Function Minimization. *Math. Comp.* **1970**, *24* (111), 647–656.
- (55) Steihaug, T. Practical Methods of Optimization Volume 1 : Unconstrained Optimization, by R. Flet-Cher, Wiley, New York, 1980, 120 Pp. Price: \$24.50. *Networks* **1982**, *12* (4), 508–509.
- (56) Bernasconi, M.; Chiarotti, G. L.; Focher, P.; Scandolo, S.; Tosatti, E.; Parrinello, M. First-Principle-Constant Pressure Molecular Dynamics. *J. Phys. Chem. Solids* **1995**, *56* (3), 501–505.
- (57) Hamann, D. R.; Wu, X.; Rabe, K. M.; Vanderbilt, D. Metric Tensor Formulation of Strain in Density-Functional Perturbation Theory. *Phys. Rev. B: Condens. Matter Mater. Phys.* **2005**, *71* (3), 035117.
- (58) Laflamme Janssen, J.; Gillet, Y.; Poncé, S.; Martin, A.; Torrent, M.; Gonze, X. Precise Effective Masses from Density Functional Perturbation Theory. *Phys. Rev. B: Condens. Matter Mater. Phys.* **2016**, *93* (20), 205147.
- (59) Hamann, D. R. Optimized Norm-Conserving Vanderbilt Pseudopotentials. *Phys. Rev. B: Condens. Matter Mater. Phys.* **2013**, *88* (8), 085117.
- (60) van Setten, M. J.; Giantomassi, M.; Bousquet, E.; Verstraete, M. J.; Hamann, D. R.; Gonze, X.; Rignanese, G.-M. The PseudoDojo: Training and Grading a 85 Element Optimized Norm-Conserving Pseudopotential Table. *Comput. Phys. Commun.* **2018**, *226*, 39–54.
- (61) Blöchl, P. E. Projector Augmented-Wave Method. *Phys. Rev. B: Condens. Matter Mater. Phys.* **1994**, *50* (24), 17953–17979.
- (62) Gonze, X.; Finocchi, F. Pseudopotentials Plane Waves–Projector Augmented Waves: A Primer. *Phys. Scr.* **2004**, *2004* (T109), 40.
- (63) Blöchl, P. E.; Jepsen, O.; Andersen, O. K. Improved Tetrahedron Method for Brillouin-Zone Integrations. *Phys. Rev. B: Condens. Matter Mater. Phys.* **1994**, *49* (23), 16223–16233.
- (64) Tantardini, C. When Does a Hydrogen Bond Become a van der Waals Interaction? A Topological Answer. *J. Comput. Chem.* **2019**, *40* (8), 937–943.
- (65) Tantardini, C.; Michalchuk, A. A. L.; Samtsevich, A.; Rota, C.; Kvashnin, A. G. The Volumetric Source Function: Looking Inside van der Waals Interactions. *Sci. Rep.* **2020**, *10* (1), 7816.
- (66) Tantardini, C.; Michalchuk, A. A. L. Dess-Martin Periodinane: The Reactivity of a Δ^5 -Iodane Catalyst Explained by Topological Analysis. *Int. J. Quantum Chem.* **2019**, *119* (6), e25838.

- (67) Fedorov, A. Yu; Drebushchak, T. N.; Tantardini, C. Seeking the Best Model for Non-Covalent Interactions within the Crystal Structure of Meloxicam. *Comput. Theor. Chem.* **2019**, *1157*, 47–53.
- (68) Tantardini, C.; Benassi, E. Topology vs Thermodynamics in Chemical Reactions: The Instability of PH S. *Phys. Chem. Chem. Phys.* **2017**, *19* (40), 27779–27785.
- (69) Tantardini, C.; Ceresoli, D.; Benassi, E. Source Function and Plane Waves: Toward Complete Bader Analysis. *J. Comput. Chem.* **2016**, *37* (23), 2133–2139.
- (70) Perdew, J. P.; Burke, K.; Ernzerhof, M. Generalized Gradient Approximation Made Simple. *Phys. Rev. Lett.* **1997**, *78* (7), 1396–1396.
- (71) Gonze, X.; Amadon, B.; Antonius, G.; Arnardi, F.; Baguet, L.; Beuken, J.-M.; Bieder, J.; Bottin, F.; Bouchet, J.; Bousquet, E.; Brouwer, N.; Bruneval, F.; Brunin, G.; Cavignac, T.; Charraud, J.-B.; Chen, W.; Côté, M.; Cottenier, S.; Denier, J.; Geneste, G.; et al. The Abinitproject: Impact, Environment and Recent Developments. *Comput. Phys. Commun.* **2020**, *248*, 107042.
- (72) Momma, K.; Izumi, F. VESTA 3 for Three-Dimensional Visualization of Crystal, Volumetric and Morphology Data. *J Appl Cryst. J. Appl. Crystallogr.* **2011**, *44*, 1272–1276.
- (73) Otero-de-la-Roza, A.; Johnson, E. R.; Luña, V. Critic2: A Program for Real-Space Analysis of Quantum Chemical Interactions in Solids. *Comput. Phys. Commun.* **2014**, *185* (3), 1007–1018.